Mechanical Characterization of Protein L in the Low-Force Regime by Electromagnetic Tweezers/Evanescent Nanometry

Ruchuan Liu,[†‡*] Sergi Garcia-Manyes,[†*] Atom Sarkar,[†§] Carmen L. Badilla,[†] and Julio M. Fernández[†*]
[†]Department of Biological Sciences, Columbia University, New York, New York 10027; [‡]Department of Physics, National University of Singapore, Singapore, 128805; and [§]Department of Neurological Surgery, Ohio State University, Columbus, Ohio 43210

ABSTRACT Mechanical manipulation at the single molecule level of proteins exhibiting mechanical stability poses a technical challenge that has been almost exclusively approached by atomic force microscopy (AFM) techniques. However, due to mechanical drift limitations, AFM techniques are restricted to experimental recordings that last less than a minute in the high-force regime. Here we demonstrate a novel combination of electromagnetic tweezers and evanescent nanometry that readily captures the forced unfolding trajectories of protein L at pulling forces as low as 10 ~ 15 pN. Using this approach, we monitor unfolding and refolding cycles of the same polyprotein for a period of time longer than 30 min. From such long-lasting recordings, we obtain ensemble averages of unfolding step sizes and rates that are consistent with single-molecule AFM data obtained at higher stretching forces. The unfolding kinetics of protein L at low stretching forces confirms and extends the observations that the mechanical unfolding rate is exponentially dependent on the pulling force within a wide range of stretching forces spanning from 13 pN up to 120 pN. Our experiments demonstrate a novel approach for the mechanical manipulation of single proteins for extended periods of time in the low-force regime.

INTRODUCTION

Owing to its remarkable ability to manipulate short recombinant proteins, single-molecule atomic force microscopy (AFM) has become a valuable tool for examining the conformational dynamics of proteins under the effect of an external stretching force with ångstrom resolution (1,2). The combination of single-protein AFM techniques with molecular engineering techniques has emerged as a novel approach to show details of the (un)folding free-energy landscape of a single protein along a well-defined reaction coordinate by tracking the protein end-to-end length over time of a great variety of proteins exhibiting different structural topologies (1,3–6,8–13).

The advent of the force-clamp spectroscopy techniques has provided direct access to the quantification of the kinetic parameters that govern the protein forced unfolding reaction, such as the unfolding rate in the absence of force and the distance to the transition state. This operational mode uses an electronic feedback system to hold a single molecule at a constant pulling force over time (14). In the case of a polyprotein, the resulting length-versus-time traces exhibit staircases in which the height of every step serves as a fingerprint for the unfolding of each particular module in the chain. An average of a few such unfolding traces therefore gives the probability of unfolding as a function of time, which can be approximated by an average unfolding rate for each stretching force. This approach has proved successful at measuring the dependency of the unfolding rate as a function of force for ubiquitin and I27, in both their polyprotein and monomeric forms (15,16). However, these two proteins exhibit a relatively high degree of mechanical stability, and therefore these studies have been limited to the high-force regime (>90 pN). Because the unfolding rate has been experimentally measured to be exponentially dependent on the pulling force (15), unfolding ubiquitin or I27 at lower stretching forces would require longer unfolding times (>1 min), where the mechanical drift compromises the feasibility of the experiments.

At the low-force regime, optical tweezers have been used extensively to study the mechanical properties and molecular dynamics of RNA and DNA molecules under a precisely defined force of a few pN, allowing for the reconstruction of their entire energy landscape (17–21). By contrast, the mechanical investigation of single proteins at the low-force regime with optical tweezers, although promising (22), has so far been limited to only three reports (22–24). Manipulating a protein with optical tweezers relies on the tethering of the protein to long DNA handles, greatly increasing the difficulties of the experiments. Moreover, these experiments are mostly limited to study proteins featuring low mechanical stability, because the unfolding forces cannot typically exceed the biotin-streptavidin unbinding force used in the attachment of the DNA handles with the polystyrene bead (24). On the other hand, magnetic tweezers offer the possibility to exquisitely manipulate single biomolecules attached to magnetic beads located inside a magnetic field, generating pulling forces up to a few tens of pN (25). Remarkably, magnetic tweezers afford a passive infinite-bandwidth force clamp over large displacements (26). However, these experiments have been restricted mainly to the study of nucleic acids and enzymes, such as DNA topoisomerase (27–29), or ATP motors (30), and no experimental work on proteins has been reported to date.

Submitted January 8, 2009, and accepted for publication January 21, 2009.

*Correspondence: sergi@biology.columbia.edu; or phylr@nus.edu.sg; jfernandez@columbia.edu

Editor: Taekjip Ha.

0006-3495/09/05/3810/12 $2.00

doi: 10.1016/j.bpj.2009.01.043

Therefore, there remains a lack of experimental evidence regarding the unfolding behavior of the same protein when pulled both in the high- and low-force regimes. Indeed, recent Go-model simulations predicted a ''rollover'' in the unfolding rate of I27 and Protein L at forces lower than 50–70 pN, suggestive of the coexistence of two independent unfolding mechanisms, the spontaneous and the forced one (31). The existence of both distinct mechanisms, manifested in the breakdown of the linearity of the logarithm of the unfolding rate as a function of force, would therefore imply an error in the determination of the unfolding rate in the absence of force from the extrapolation of the force-dependent unfolding rate plot in the high-force regime under force-clamp conditions (32). To experimentally bridge both force regimes, a protein with intermediate mechanical stability is required, together with a technique capable of working under force-clamp conditions at forces of a few pN in a drift-insensitive environment, permitting single protein recordings that last several minutes.

In this study, we show that the combination of single-molecule force-clamp AFM and electromagnetic tweezers-based evanescent nanometry technique explores, for the first time, a wide spectrum of unfolding forces for the small Protein L, spanning from ~10 pN to ~120 pN. The ability of electromagnetic tweezers to pull magnetic-fluorescent beads inside a field of total internal fluorescence (TIRF) microscope can be effectively used to study the folding/unfolding dynamics of a short engineered polyprotein made of eight repeats of protein L. In this instrument, the TIRF field serves as a precise locator of the vertical position of a protein-coated magnetic-fluorescent bead. This technique, called evanescent nanometry, can optically detect the changes in length or position of a single molecule attached to the bead moving along the z axis of an optical microscope, with subnanometer length and millisecond time resolution (33). By applying current to an electromagnet, a calibrated pulling force is applied to the paramagnetic-fluorescent bead. As the attached polyprotein unfolds in steps under the constant pulling force, the bead itself moves upward away from the surface. A recording of the bead's fluorescence signal as it moves through the evanescent field is therefore an accurate reporter of the protein extension over time when pulled under a constant force of a few pN.

The 62 residue IgG binding domain of peptostreptococcal protein L consists of a four-stranded β-sheet packed against a single α-helix. Protein L has been used widely as a model of single-domain protein folding, and the kinetics and thermodynamics of folding/unfolding protein L have been extensively characterized by chemical (34–36) and thermal (37) denaturation at the bulk level, and by fluorescence resonance energy transfer measurements (38,39) at the single-molecule level. Although it has no known mechanical function, protein L was shown to be mechanically resistant using single-molecule AFM (40). Even though Protein L is topologically similar to ubiquitin, it features a much lower mechanical stability than ubiquitin or I27. Therefore, because of its intermediate mechanical properties, Protein L exhibits an unfolding force range that covers both the high-force region (>80 pN), which can be probed by AFM, and the low-force region (close to 10 pN), which can be explored with electromagnetic tweezers, revealing itself as the ideal candidate to experimentally bridge the (so-far-elusive) force gap.

MATERIALS AND METHODS

Protein engineering

The polyprotein used in this study (Protein L)$_8$ was engineered by consecutive subcloning of the Protein L monomers using the *Bam*HI and *Bgl*II restriction sites (41). The plasmid containing the B1 immunoglobulin binding domain of peptostreptococcal Protein L (35) was a generous gift from Professor David Baker (University of Washington). The eight-domain Protein L was cloned into the pQE80L (Qiagen, Valencia, CA) expression vector and transformed into the BLR DE3 *Escherichia coli* expression strain. The engineered polyprotein L construct contains 12 extra residues in the C-terminus (MRGSHHHHHHGS-) and four extra residues in the N-terminus (-RSCC). Two neighboring protein monomers are separated by two residues, namely -RS- (16). The polyprotein construct was purified by histidine metal-affinity chromatography with Talon resin (Clontech, Mountain View, CA) and by gel filtration using Superdex 200 HR column (GE Bio-Sciences, Piscataway, NJ).

Force-clamp spectroscopy with AFM

Force-clamp AFM experiments are conducted using a homemade set-up under force-clamp conditions as described elsewhere (15,43). The sample is prepared by depositing 1–10 μL of protein (1–10 μg mL^{-1}) onto a freshly evaporated gold cover slide. Each cantilever (Si_3N_4 Veeco MLCT-AuHW) is individually calibrated using the equilibration theorem (44), giving rise to typical spring constant values of 20 pN nm^{-1}. Single polyproteins are picked up from the surface by pushing the cantilever onto the surface and exerting a contact force of 500–800 pN to promote the nonspecific attachment of the proteins to the cantilever tip surface. The cantilever actuator is then retracted to produce a set deflection (force), which is kept constant throughout the experiment thanks to an active feedback mechanism while the protein extension is recorded. The force feedback is based on a proportional, integral, and differential amplifier whose output is fed to the piezoelectric positioner. The feedback response is limited to 3–5 ms. Our measurements of protein length have a peak-to-peak resolution of ~0.5 nm.

Data analysis

All data were recorded and analyzed using custom software written in Igor Pro 5.0 (Wavemetrics, Lake Oswego, OR). For the unfolding kinetics study, only traces with $\geq$6 unfolding events with long detachment times were analyzed. We summed and normalized ~10–80 unfolding recordings obtained for each pulling force. To obtain the unfolding rate at each particular force, we fitted these averaged traces with single exponentials. To estimate the error on our experimentally obtained rate constants, we carried out the nonparametric bootstrap method. At a given value of force, n unfolding staircases were randomly drawn with replacement from our original data set. These were summed and fitted to obtain a rate constant. This procedure was repeated 500 times for each data set, resulting in a distribution that provided the standard error of the mean corresponding to the unfolding rate of the native (Protein L)$_8$.

Chemical functionalization of glass substrates and fluorescent magnetic beads

Glass coverslides (Thermo Fisher Scientific, Pittsburgh, PA) were functionalized by incubating them with a solution containing 100 mg mL^{-1}

methoxy-polyethylene glycol-succinimidyl propionate (mPEG-SPA; Nektar Therapeutics, Huntsville, AL) and 10 mg mL^{-1} succinimidyl α-methylbutanoate-polyethylene glycol- succinimidyl α-methylbutanoate (SMB-PEG-SMB; Nektar Therapeutics) in 0.1 M phosphate buffer for 2 h. Application of ~1 nM poly-protein L solution in HEPES buffer for 1 h allowed the covalent linkage of the polyprotein to the surface-bound SMB functionalized PEG. Finally, a mixture containing 20 mg mL^{-1} *N*-(3-Dimethylaminopropyl)-*N*′-ethyl carbodiimide hydrochloride (Sigma, St. Louis, MO), 10 mg mL^{-1} *N*-hydroxysulfosuccinimide sodium salt (Fluka, St. Louis, MO), and 0.1% (w/v) paramagnetic fluorescent beads (2.3 μm; Spherotech, Lake Forest, IL) promoted the covalent linkage between beads and the surface-bound $(\text{protein L})_8$.

Combined magnetic tweezers and TIRF microscope

The combined force and fluorescence microscope was built on the basis of the set-up described elsewhere (33) by replacing the previous AFM head (Fig.1 *a*) with a home-built electromagnet system (Fig. 1 *b*). The electromagnet system consists of a 5 mm wide iron rod core (Alfa Aesar, Ward Hill, MA), fashioned to a 45° cone-shaped end and wrapped with 130 ft of 16 AWG Heavy-Armored Poly-thermaleze magnet wire (Belden, Richmond, IN), resulting in a solenoid of 35 mm in height and 55 mm in diameter. The electromagnet was contained in a customized aluminum case. To remove heat, the aluminum housing was equipped with a central motor-oil-filled core and a surrounding series of channels that allowed water-mediated cooling of the apparatus. An XFR 1.2 kW 20–60 DC power supply (Xantrex Technology, Burnaby, Canada) was connected to the electromagnet and the current mode of the power supply provided a simple way to set any output current. The electromagnet head is mounted onto a 30-mm-thick aluminum base plate via a *z* translator (Spectra-Physics, Mountain View, CA) bolted onto an aluminum tower. Data acquisition and control of instrumentation are done by means of data acquisition card (6052E, National Instruments, Austin, TX) controlled by software written in Igor Pro 5.0 (WaveMetrics, Lake Oswego, OR). In addition to being a physical mount for the electromagnet, the base plate is also the stage for the TIRF microscope and contains a cutout for the Olympus APO 60×/1.45 oil immersion lens. All studies were carried out by generating an evanescent wave with a 488-nm argon ion laser (IMA 100, Melles Griot, Irvine, CA), using the "through-the-lens" method. The emitted light was passed through a green filter set consisting of a 505-nm dichroic mirror and a 510-nm long-pass filter (Chroma Technology, Rockingham, VT), and collected by an iXon DV887 back-illuminated electron-multiplying charge-coupled device (EMCCD) (512 × 512 pixels, 16 × 16 μm per pixel, with 95% quantum efficiency) operated at −60°C with a 5-MHz readout rate. All fluorescence data were normalized to their maximum value. The EMCCD camera is controlled by custom-made external operation (XOP) functions that were controlled by the main Igor Pro program.

Calibration of the penetration depth of the evanescent field

Calibration of the TIRF microscope was carried out by making use of our set-up described previously (33), which relied on the combination of the TIRF microscope with a piezoelectric actuator to achieve spatial nanometer resolution in the *z* direction. According to the procedure described in (33), a 2.3 μm paramagnetic fluorescent bead is glued to the tip of an AFM cantilever, which in turn is glued to a piezo actuator. The actuator is on the aluminum base plate, and is exchangeable with the electromagnet head. The scheme of this set-up is shown in Fig. 1 *a*. The calibration of the evanescent field has been discussed in detail previously (33), and relies on using the *z* piezo actuator to drive a fluorescent bead through an evanescent field. The stability and high spatial sensitivity of the evanescent field makes it an ideal tool for measurement of the bead displacement in the *z* direction over a wide range of distances spanning from a few nanometers up to a few micrometers. Fig. 1 *c* shows typical evanescent field calibrations with different penetration depths using a 2 μm bead. Because the polyproteins used in the experiments exhibit full extensions around 160 nm, TIRFM fields with penetration depths of ~150 ~ 200 nm were typically chosen.

Electromagnetic tweezers force calculation and calibration

The force *F* applied on the paramagnetic beads, created by the field generated by the electromagnetic tweezers, can be calculated according to the relationship

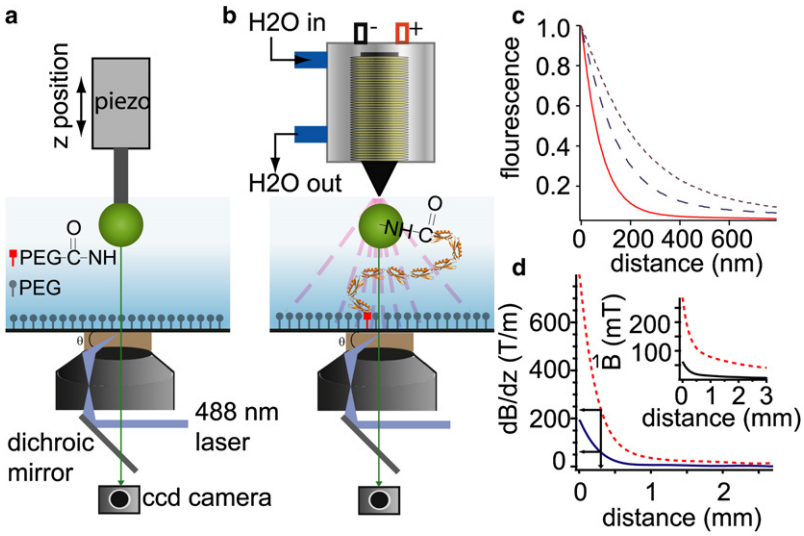

FIGURE 1 Single polyproteins can be unambiguously unfolded using a combination of electromagnetic tweezers and evanescent nanometry. (*a*) Scheme of the experimental set-up used to calibrate the penetration depth of the evanescent field generated by the TIRF microscope. The calibration protocol relies on a fluorescent magnetic bead attached to a *z* piezoelectric actuator that is mounted on top of the microscope. The fluorescence intensity of the bead is collected by an EMCCD camera. The position of the fluorescent bead along the vertical, *z*-direction is measured by the TIRF-generated evanescent wave. Because the intensity of the evanescence field decays exponentially with the vertical distance, the fluorescence intensity of the bead moving through the evanescent field can be easily translated into real distance with nm resolution, as observed in the calibration curve shown in *c*. (*b*) Scheme of the experimental set-up consisting of a combination of the TIRF microscope with a custom-built, water-cooled, electromagnetic head mounted on top of the microscope. During the experiment, each polyprotein molecule is tethered between the polyethylene glycol-functionalized glass surface and a fluorescent paramagnetic magnetic bead. When a current is applied to the magnet, the generated magnetic field exerts a constant pulling force on the paramagnetic bead. As the attached polyprotein unfolds, the bead moves upward, away from the surface. The movement of the protein-bead system can be precisely tracked by recording the fluorescence signal of the bead as it moves through the evanescent field. (*c*) Calibration curve that relates the fluorescence intensity of the fluorescent bead with the interface of the TIRF microscope at different incident angles. The fluorescence signal decays exponentially with the distance. In the example, tunable decay depths (d_p) of 80 nm (*solid line*), 146 nm (*dashed line*), and 231 nm (*dotted line*) are obtained. (*d*) Calibration curve (*inset*) of the magnetic field generated by the magnet as a function of the distance from the tip of the magnet. Calibrating the gradient of the magnetic field with the distance at different current intensities of 20 A (*dashed line*) and 3 A (*solid line*) allows one to calculate the force experienced by the bead according to Eq. 1 in the text.

$$F = \frac{dB}{dz} \times m_{\text{dipole}}, \quad (1)$$

where dB/dz is the vertical (z) gradient of magnetic field, and m_{dipole} is the magnetic dipole of the paramagnetic bead in the magnetic field B. A Gauss meter (Model 410, Lake Shore Cryotronics, Westerville, OH) was used to measure the magnetic fields generated by the electromagnet with respect to the distance from the tip of the magnet (Fig. 1 *d*, *inset*). The gradient of the magnetic field versus distance can therefore be directly calculated from the field measurement. Fig. 1 *d* shows a typical curve of dB/dz versus the distance from the electromagnetic tip at currents of 3 A (*solid curve*) and 20 A (*dashed curve*). The value of m_{dipole} depends on the magnetic field, and it is estimated from the magnetic hysteresis loop of the magnetic beads provided by the manufactory (Spherotech). In a typical experiment, the distance of the electromagnet tip to the sample is set around 300 ~ 550 μm. According to these values, the force exerted on the bead can be calculated to be in the range of 13 pN ~ 36 pN when using a current of 20 A and 1.1 pN ~ 4.4 pN when using a current of 3 A.

In our experiments the movement of beads is restricted to only ~160 nm according to the protein's maximal extension. For such a small range of distances, the change in the magnetic field is negligible, such that the applied force is kept constant throughout the experiment without the need for external feedback loops (26). Therefore, for the same rationale, small changes in distance due to mechanical drift do not have any effect on the applied force, which makes our force-clamp technique insensitive to drift. In our experiments we used a 100 mW laser (λ= 488 nm). However, the effective laser intensity on the sample is significantly reduced after passing through the optics of the microscope and forming the evanescent field. We do not know the actual intensity at the bead's position inside the evanescent field. However, photobleaching of the bead is not a significant problem ($\leq$5%), even over the extended timescales of our experiments. Photobleaching would not affect the force applied to a polyprotein, only the measured length. If the bead suffered significant photobleaching, the polyprotein length would change over time, reducing the size of the elongation of protein L on unfolding. Our data shows that typically, the maximal elongation of an unfolded polyprotein remains constant over >30 min. Our traces of length (intensity) versus time do not show upward/downward trends; if they did, they were not considered in the analysis.

Force calibration in situ

The majority of the work reported using magnetic tweezers is done with long molecules of DNA or RNA, usually using permanent magnets. In these cases, where the distance between the surface and the magnetic bead is of several microns, the prevailing force calibration is based on the measurement of fluctuations in the x-y plane (26). By contrast, in our experiments, the length of a folded polyprotein plus the PEG linker is shorter than ~70 nm. At a low pulling force of ~10 pN, the variance of the fluctuations in the x-y plane are expected to be small (<10 nm^2), which are difficult to resolve in the x-y plane, but much easier to detect in the z direction, as we show here.

To calibrate force in situ, we devised a protocol that takes advantage of the nanometer resolution of measurements in evanescent nanometry (33) and the ability to rapidly ramp force by the current delivered to the electromagnetic tweezers. Our protocol is shown in Fig. 2 *a*. The bead-molecule system is first stretched at a maximal current I (Fig. 2 *a*, *bottom curve*,) for 45 s to fully extend the molecule. Then, the current is ramped down linearly from I to a minimal current I_0, and subsequently ramped back up again by increasing I_0 back to I at a frequency of 0.25 Hz. Such a cycle is repeated 50 times. The z extension of the molecule (Fig. 2 *a*, *top curve*) is obtained by monitoring the intensity of bead fluorescence in the TIRF microscope according to:

$$z = d_p \times \ln\left(\frac{FL_{\max}}{FL}\right), \quad (2)$$

where d_p is the penetration depth from evanescent nanometry calibration, FL is corresponding fluorescence intensity and $FL_{\max}$ is the maximum fluorescence intensity. A cumulative plot of the extension of the bead-protein system as a function of the applied current (Fig. 2 *b*, *dots*) is fitted to a polynomial function (Fig. 2 *b*, *solid line*). It is noteworthy that the saturation of the extension of the bead-protein system at current values $\geq$10 A results from the working conditions of our electromagnet. Therefore, the observed saturation is not related to the elastic behavior of the stretched protein. From the differences between each point in Fig. 2 *b* and the polynomial fit, the variance in z extension, $\langle \sigma_z^2 \rangle$, is obtained.

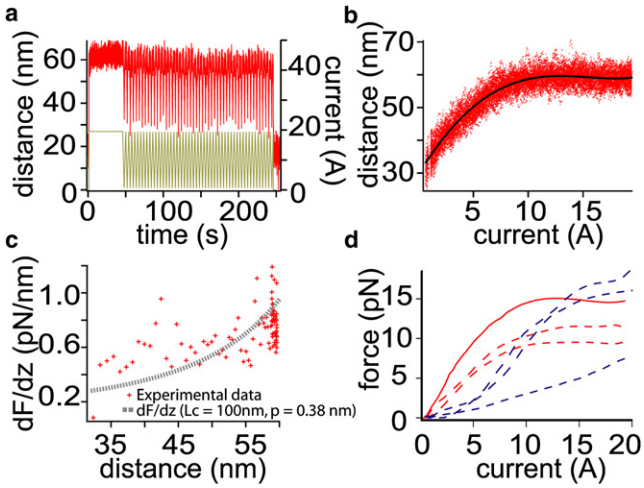

FIGURE 2 The fast current ramp protocol for in situ force calibration of electromagnetic tweezers. (*a*) The z distance of the fluorescent magnetic bead is recorded (*top curve*) while the current of electromagnet is ramped in cycles of 4 s from 20 A to 0.1 A and back up to 20 A (*bottom curve*). (*b*) A cumulative plot of distance versus current (*dots*) from all cycles in *a* is fitted to a polynomial (*solid line*). (*c*) The force gradient versus distance is calculated from the variances in distance in *b*. A combined protein + linker tandem exhibiting a contour length of L_c = 100 nm and a persistence length of p = 0.38 nm can be modeled by the WLC model of polymer elasticity yielding a stiffness trend that, overall, reproduces the experimental data (*dashed line*). (*d*) The relationship between force and current obtained by integration of force gradient; the solid curve is calculated from *c*, and the dashed curves represent calibrations of different beads at different positions.

During the current ramp, provided no unfolding/refolding events take place, the system is very close to thermal equilibrium, so the equipartition theorem for Gibbs ensemble can be applied, using the gradient of the force versus extension (2,46):

$$\frac{dF}{dz} = \frac{k_B T}{\langle \sigma_z^2 \rangle_{\text{thermal}}}, \quad (3)$$

where k_B is Boltzmann constant, T is temperature in Kelvin, k_BT is the thermal energy, and F is the force on the bead.

Using Eq. 3, we can calculate the stiffness (dF/dz) of the bead-protein system as a function of the distance z (Fig. 2 *c*). The measured stiffness agrees with that calculated from the worm-like chain model of polymer elasticity using values of contour length L_c = 100 nm and persistence length p = 0.38 nm (Fig. 2 *c*, *dashed line*).

Some of the deviations may be due to the effects of viscous drag on the beads (~2–3 μm in diameter) that operate close to the surface and limit the bandwidth of the thermal fluctuations measured in the z direction.

To estimate the pulling force, F, Eq. 3 can be integrated:

$$F = \int_{z(I_0)}^{z(I)} \frac{k_B T}{\langle \sigma_z^2 \rangle_{\text{thermal}}} dz(I) + F(I_0), \quad (4)$$

where I and I_0 are the actual and lowest currents applied to the electromagnet. Typically, I_0 is kept slightly above zero (e.g., 0.5 A) to prevent

the bead from touching the surface. To apply it to our discrete data set, Eq. 4 is converted into a sum:

$$F = \sum_{I_0}^{I} \frac{k_B T}{\langle \sigma_z^2 \rangle_{thermal}} \Delta z(I), \quad (5)$$

where $\Delta z(I)$ is the change in extension for each current increment, ΔI. The calibration results show that the electromagnetic force on the beads increases with the input current and saturates at high currents (Fig. 2 *d*), which we believe is due to saturation of magnetization of either or both the beads, and the iron core of the electromagnet. Our calibrations show forces of 13 ± 4 pN at a current of 20 A and 3 ± 2 pN at a current 3 A. These calibrated forces are consistent with the range of forces calculated from the measurements of the magnetic gradient (Eq. 1). The acquisition frequency of our camera is 400 Hz. Owing to Nyquist, this limits the bandwidth of our fluorescent measurements to <200 Hz. This limited bandwidth may be suppressing high frequency fluctuations of the bead-polyprotein system, reducing the magnitude of the measured variance during the force calibration. According to Eq. 5, this may result into an overestimate of the pulling force. In these experiments the camera shot noise makes a negligible contribution. In contrast to the detection of single-molecule fluorescence, the beads used in our experiments allow for a large fluorescence signal, which reports length without being influenced by the noise of the camera. Our length calibration curves show that camera noise causes an uncertainty in the length that is <1 nm (33).

RESULTS

Step height as a fingerprint for protein unfolding at a constant force

Force-clamp traces of polyproteins give rise to staircase patterns in which the height of each step corresponds to the number of amino acids released on unfolding a single module in the chain at a constant force (14). Working with concatamers unambiguously distinguishes between the spurious interactions between the bead or the cantilever tip with the surface and the length trajectories resulting from stretching the polyprotein (16,41). For a given protein, the step height is expected to increase with the pulling force, as described by the worm-like chain model of polymer elasticity (WLC), where only entropic contributions of the chain are considered. In our experiments, the $(\text{Protein L})_8$ polyprotein is held at a constant pulling force, either using a paramagnetic bead placed in a electromagnetic field (Fig. 3 *a*) in the case of the magnetic tweezers set-up, or using a cantilever tip under a constant deflection in the AFM (Fig. 3 *b*). The length-versus-time trajectories in both cases yield a similar stepwise protein elongation pattern as each module of the chain unfolds. When the polyprotein is stretched at ~13 pN by the electromagnetic field, we observe a step height of ~11 nm (Fig. 3 *c*), whereas when the protein is pulled at higher forces (~60 pN) with the AFM tip, the measured step size increases up to ~15 nm (Fig. 3 *d*). From the average of an ensemble of individual trajectories such as those shown in Figs. 3 *c–d* at each particular pulling force, we aim to measure the average unfolding rate and the corresponding step height distribution. Although single-molecule force-clamp spectroscopy with AFM has already established itself as a robust technique for studying mechanically resistant proteins under constant force, there is a need to develop experimental techniques able to probe the low-force regime of proteins exhibiting mechanical stability.

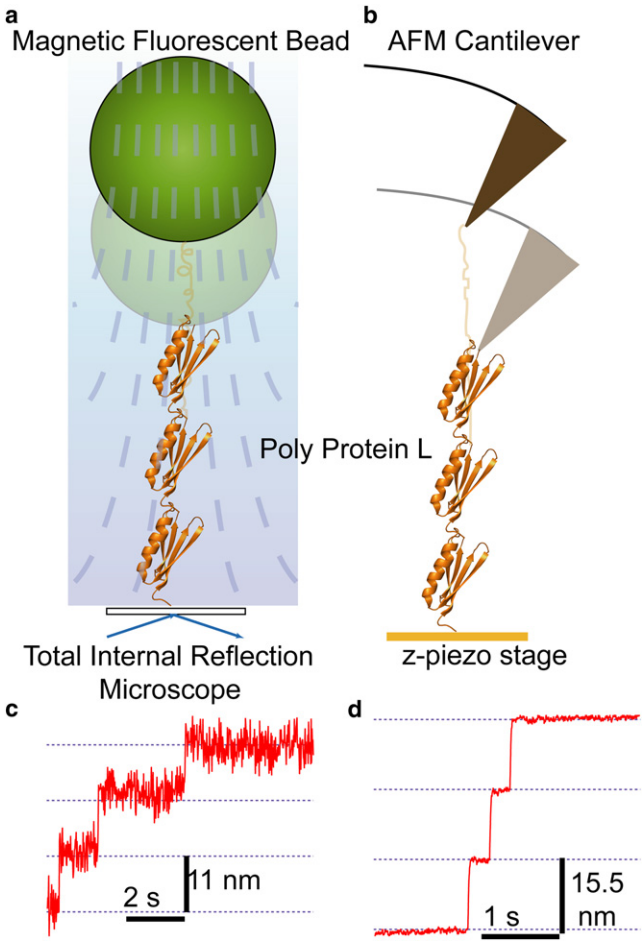

FIGURE 3 Unfolding polyProtein L under force-clamp conditions yields staircase patterns in which each step corresponds to the unfolding of one module in the chain. Scheme of the experimental set-up, in which a single polyprotein is stretched at constant force (*a*) by a magnetic fluorescent bead placed in an evanescent field, or (*b*) by a cantilever tip of an AFM set-up working under constant-force conditions. Typical length-versus-time recordings corresponding to the unfolding of a Protein L polyprotein when pulled (*c*) at~13pN by electromagnetic tweezers, or (*d*) at ~60 pN when stretched by force-clamp AFM . In both cases, the protein elongates in steps featuring equal height.

Exploring the low-force unfolding regime of $(\text{Protein L})_8$ by electromagnetic tweezers

In a previous study (33), we showed the capability of the so-called ''evanescent nanometry technique'' to detect the changes in length of a single molecule moving along the *z* direction of an optical microscope, with subnanometer and millisecond time resolution. This approach relies on a TIRF-generated evanescent wave to measure the position of a fluorescent particle moving along the *z* axis. Because the intensity of the evanescent wave decays exponentially

with the vertical distance, it can be used as a precise way to translate fluorescence intensity into length with nanometer resolution. In these early experiments, the TIRF instrument was combined with an AFM to pull a polyprotein through the evanescent field. Although viable, these experiments encountered the drift problems associated with the AFM apparatus. To eliminate such mechanical drift, we have now improved this technique by building a water-cooled electromagnet with a sharp soft iron core tip that creates large magnetic gradients up to 450 mT/mm. The tip of the magnet is placed near the surface of the TIRF microscope. Application of a controlled current to the magnet generates a magnetic gradient that exerts a defined force to the paramagnetic bead, pulling the bead straight through the evanescent field. On the application of a constant force, the protein L polyprotein, tethered between the functionalized glass coverslide surface and the bead, unfolds in a stepwise manner with the concomitant movement of the bead upward away from the surface. The movement of the protein-bead tandem in the *z*-direction can be then precisely tracked by recording the fluorescence signal of the bead as it moves through the evanescent field. A scheme of the experimental set-up is shown in Fig. 1 *b*.

The application of different current protocols to the magnet allows for the study of different length-force relationships, similar to the standard protocols used in force-clamp spectroscopy with AFM (2,15,43). In the most simple experiment (Fig. 4 *a*), a constant current of 20 A is applied to the magnet during 10 s (*top trace*). On the application of force, the bead is pulled away from the surface, as observed by the sudden drop in the fluorescence intensity (*middle trace*). During the next ~5 s, the fluorescence intensity of the bead decreases in a stepwise manner, indicating that the bead is pushed away from the surface as the protein unfolds. This is observed in the concomitant length-versus-time recording (*bottom trace*), which mirrors the descending staircase observed for the fluorescence intensity signal. This experiment unambiguously shows the success of evanescent nanometry in following the unfolding pathway of a single protein under a constant force of a few picoNewtons. Fig. 4, *b* and *c*, show the time evolution of the stepwise decay (increase) in fluorescence (length) once a current is applied to the magnet after a ramp (Fig. 4 *b*) or a quench (Fig. 4 *c*) protocol. A precise in situ calibration of the current-force relationship for each individual stretched molecule is thus of extreme importance to accurately assess the force under which the protein unfolds when placed inside the evanescent field (see Materials and Methods).

The introduction of a high-power magnet to control the force at which the protein-bead tandem is pulled allows us to overcome the drift constraints that limit AFM experiments to recordings that last less than a minute. Using the combination of electromagnetic tweezers and evanescent nanometry, we readily capture the unfolding/refolding cycle of the same polyprotein for a period of time longer than 1 h at a pulling force of ~13 pN (Fig. 5). In this experiment, a current pulse of 20 A during 30 s, which exerts a calibrated pulling force of ~13 pN on the bead, triggers the polyprotein unfolding, marked by the stepwise increase in the protein length (Fig. 5, *a* and *b*, *solid curves*). The applied current (force) is subsequently quenched to zero for 60 s, allowing the protein to collapse onto its folded length. During this period of time, the protein refolds into its native conformation, as confirmed by the presence of a staircase of 10 nm steps, characteristic of the fully refolded protein L, once the current is again increased back to 20 A. Such a force quench protocol was successfully used to monitor the folding trajectories of a single ubiquitin protein, albeit at a higher force (43). The novel approach presented here extends the capability of force-quench experiments by probing the unfolding/refolding cycle process at lower unfolding forces on a much extended timescale of up to 1 h. Remarkably, unfolding steps are observed in all cycles, even after 30 min, indicating that the same protein is able to undergo multiple refolding cycles without experiencing noticeable fatigue. The unfolding regions of different traces (Fig. 5 *a*, *four boxes*) are shown in detail in Fig. 5 *b*. A histogram of all unfolding steps ($n = 75$) for the same molecule over the time course of 1 h is shown in Fig. 5 *c*. Gaussian fit to the histogram (*dashed line*) gives rise to a step height of 9.7 $\pm$ 2.7 nm.

Unfolding kinetics of protein L

Fig. 6 shows individual unfolding trajectories of a $(\text{Protein L})_8$ polyprotein when pulled under a constant stretching force by means of a force-clamp AFM in the force regime ranging from 120 pN to 40 pN (Fig. 6, *a–d*) or by the electromagnetic tweezers at ~13 pN (Fig. 6, *e* and *f*). The normalized average of an ensemble of a few of such trajectories gives the probability of unfolding as a function of time, $P(t)$, for each particular force (Fig. 6 *g*). As a first approximation, we use single exponential fits to the average time course of unfolding at each particular force to describe the average rate of unfolding of Protein L. As we have shown before in the case of ubiquitin, a single exponential fit captures ~81% of the unfolding events and thus represents a reasonable measure of the unfolding rate even when the native state is composed of an ensemble of structures of slightly different energies (47,48). For other proteins such as Protein G, a single exponential fit seems to describe even better the unfolding rate at each particular force, suggesting that the native state of protein G is a unique, well-defined structure (49). Although the characterization of roughness in the native state of protein L is far from the scope of this study, the single exponential fits to the data shown in Fig. 6 *g* provide a very good approximation to experimentally measure the unfolding rate within the entire range of pulling forces spanning from 13 pN up to 120 pN. From Fig. 6 *g*, it is evident that the protein L unfolding rate is strongly dependent on the pulling force. We have shown recently that the force-dependent unfolding rate of polyubiquitin and polyI27 can be approximated by the simple Bell model (15,16,50,51),

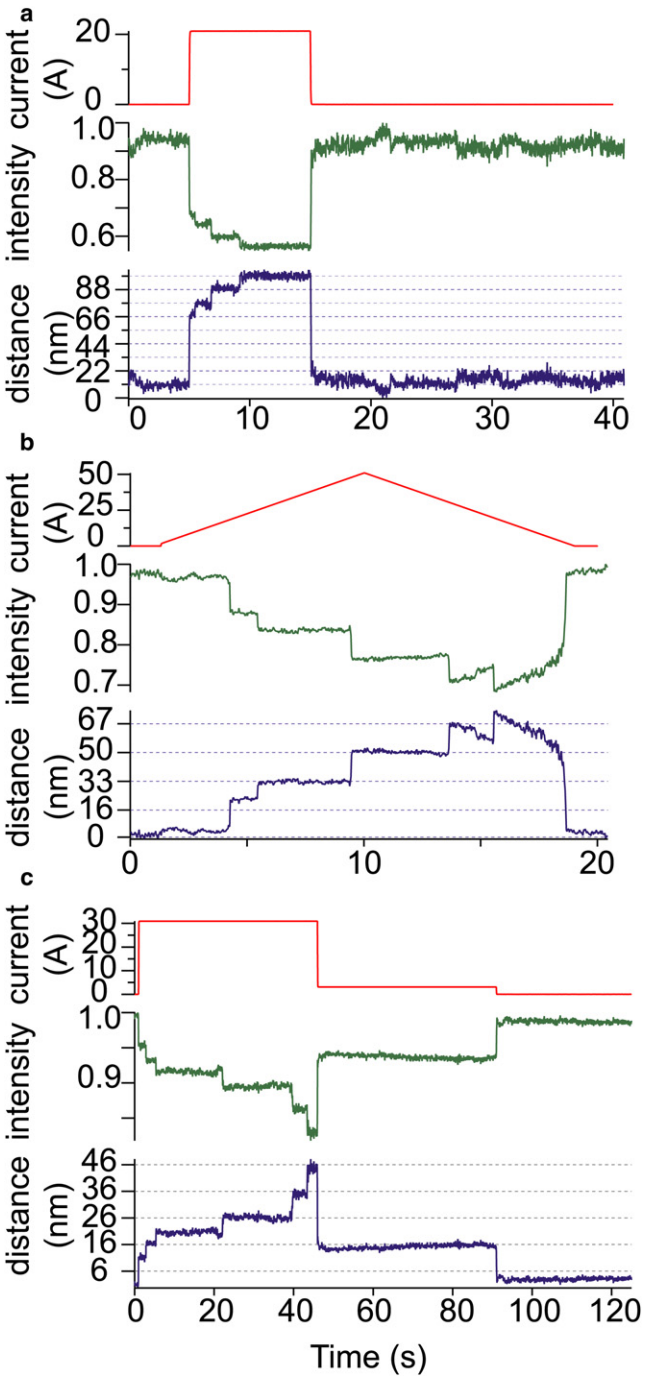

FIGURE 4 Using different current (force) protocols, we monitor the unfolding and folding trajectories of a (Protein L)$_8$ polyprotein by tracking the evolution of the fluorescence intensity of the bead-protein system over time. (*a*) When a constant current of 20 A is applied to the magnet during 10 s (*top trace*), a stepwise decrease in fluorescence intensity (arbitrary units) of the paramagnetic bead is observed (*middle trace*), indicating that the bead has moved upward from the surface as the attached protein unfolds. Because the fluorescence intensity can be accurately translated into vertical distance with nanometer resolution (see Materials and Methods), the corresponding length-versus-time recording (*bottom trace*) monitors the unfolding trajectory of Protein L. (*b*) In a force-ramp protocol, the current is linearly increased to 50 A during 10 s, resulting in a staircase of diminishing amplitude in the fluorescence intensity signal. The concomitant length-versus-time trace shows the polyprotein unfolding trajectory, exhibiting in a stepwise increase in protein length. After 10 s, the current (force) is linearly decreased to 0 A during 10 s, triggering the protein to collapse into its folded length, as revealed by the cooperative decrease (increase) in length (fluorescence intensity). (*c*) Experimental folding trajectory of a Protein L polyprotein obtained by using a two-pulse protocol. A first current pulse of 30 A is applied to the magnet during 45 s, which results in the unfolding of the protein as marked by the stepwise increase in length. After this period of time, the current (force) is quenched down to 3 A, triggering the protein to collapse into its folded length in the millisecond timescale.

which pictures the unfolding reaction as a two-state process limited by a well-defined energy barrier, the height of which is modulated by the stretching force according to the relationship

$$\alpha(F) = \alpha(0)\exp(F\Delta x/kT), \quad (6)$$

where F is the pulling force, $\alpha(0)$ is the rate constant in the absence of force, and Δx is the distance to the transition state. The linear relationship observed in the semilogarithmic plot of the unfolding rate of Protein L as a function of the pulling force (Fig. 7 *a*) directly shows that the unfolding rate of Protein L is also exponentially dependent on the pulling force. The fit of Eq. 6 to the experimental data shown in Fig. 7 *a* gives values of $\Delta x = 1.5 \pm 0.1$ Å and $\alpha(0) = 0.067 \pm 0.019$ s^{-1}. Previous results on ubiquitin and I27 were restricted to the high-force regime because of the drift limitations of the force-clamp AFM set-up in the long-lasting recordings at low stretching forces. The use of electromagnetic tweezers/evanescent nanometry technique allows us now to expand the regime of forces amenable to study in the force-clamp AFM. Interestingly, the unfolding rate of protein L at forces as low as 13 pN falls on the straight line of the fit of Eq. 6, in conformity with the Bell model, thereby excluding the presence of curvature in the plot of the unfolding rate as a function of the force (31).

The step height distribution as a function of the pulling force is consistent with the range of persistence length values obtained from force-ramp experiments

As stated above, our experiments rely on the presence of equally spaced steps as the unambiguous fingerprint for protein unfolding. For a given protein, the step height is expected to increase with the pulling force according only to the WLC model of polymer elasticity. Fig. 7 *b* shows the average step height corresponding to the traces analyzed in Fig. 7 *a* as a function of the pulling force. As observed in the figure and also in the experimental recordings shown in Fig. 6, *a–f*, the unfolding step size increases with the pulling force, saturating at forces >60 pN. From the fit of the WLC model of polymer elasticity (*solid line*) to the data, we obtain a contour length of $L = 18.6$ nm and a persistence length of $p = 0.58$ nm. These results are in agreement with the results obtained from constant velocity data for protein L (40). The

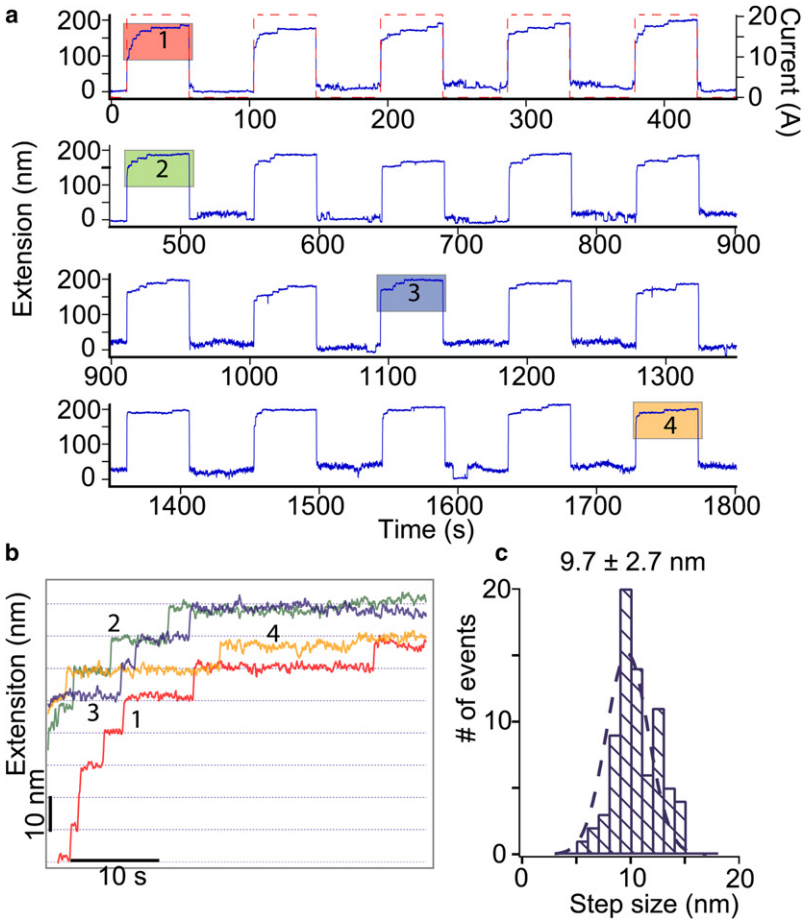

FIGURE 5 The combination of electromagnetic tweezers and evanescent nanometry allows us to capture the unfolding/refolding cycle of the same polyprotein for a period of time >1 h by applying a cyclic force-quench protocol. (*a*) Using a force-quench protocol, a first current pulse of 20 A (*dashed line*) is applied to the magnet during 30 s, exerting a constant force of ~13 pN to the bead-protein system. The application of such low pulling force results in the polyprotein unfolding, marked by the stepwise increment in length (*solid line*). Subsequently, the current intensity (force) is removed for 60 s to trigger folding. During this time, the protein recovers its native conformation, as confirmed by the presence of a staircase of 10 nm steps, characteristic of the fully refolded protein, once the current is increased back to 20 A. The same protocol is repeatedly applied to the same protein, tethered between a chemically functionalized glass cover slide and a paramagnetic fluorescent bead, for a period of time >1 h. (*b*) A detailed view of the unfolding region of different cycles from the shaded trajectories in *a*, showing the presence of unfolding steps even after 30 min that indicate that the protein is able to undergo multiple refolding cycles without exhibiting noticeable mechanical fatigue. (*c*) Histogram of all unfolding steps ($n = 75$) for the same molecule over a time course of 1 h. Gaussian fit to the histogram (*dashed line*) gives rise to a step height of 9.7 ± 2.7 nm, in agreement with the solid circle in Fig. 7 *b*.

obtained value for the persistence length ($p = 0.58$ nm) agrees with the results obtained from constant velocity data obtained in AFM for several proteins ($p \approx 0.4$ nm). Remarkably, we have recently shown from force-ramp experiments in combination with molecular dynamics simulations that a single persistence length value does not capture the mechanical behavior of all collapsing proteins; instead, a wide range of persistence length values spanning from $p = 0.4$ nm up to $p = 1.2$ nm captures the overall conformational diversity (53). Akin to the variability of persistence length values observed in our force-ramp trajectories, the distribution of step heights observed for the unfolding of protein L cannot be described by a single value. The distribution of step heights at three different pulling forces (13 pN, 40 pN, and 100 pN) is shown in Fig. 7 *b*, *inset*. Interestingly, the step height distribution is much broader at lower unfolding forces (13 pN) and narrows as the pulling force is increased. This trend is manifested in the error bars of Fig. 7 *b*. The fit of the WLC to the experimental data in which the persistence length is constrained to $p = 0.4$ nm up to $p = 1.2$ nm (*dashed lines*) defines a shaded region in Fig. 7 *b* that contains the expected step height distribution as a function of the pulling force using the extreme values of persistence length obtained from the force-ramp experiments. Remarkably, the distribution of step heights at each particular force falls within the shaded region, highlighting the consistency of the results obtained here for the unfolding process of protein L with the earlier results obtained by force-ramp experiments.

DISCUSSION

The experiments presented in this study show the success of electromagnetic tweezers in exploring the low-force regime of the unfolding free-energy landscape of a mechanically stable protein, using a novel experimental set-up that does not rely on the attachment of the protein to long handles and that does not use an external feedback electronic system to apply a constant pulling force to the studied protein. As shown in Fig. 7 *a*, the forced unfolding of protein L follows an exponential relationship within a range of pulling forces spanning from 13 to 120 pN, showing that even at a pulling force as low as 13 pN the unfolding pathway is mainly governed by the force-accelerated mechanism. However, this result does not preclude thermally activated pathways from competing with the forced-unfolding mechanism at even lower forces or, alternatively, at higher temperatures, which certainly invites experimental verification. These results are in further contradiction with the presence of a rollover in the logarithmic plot of the unfolding rate as a function of

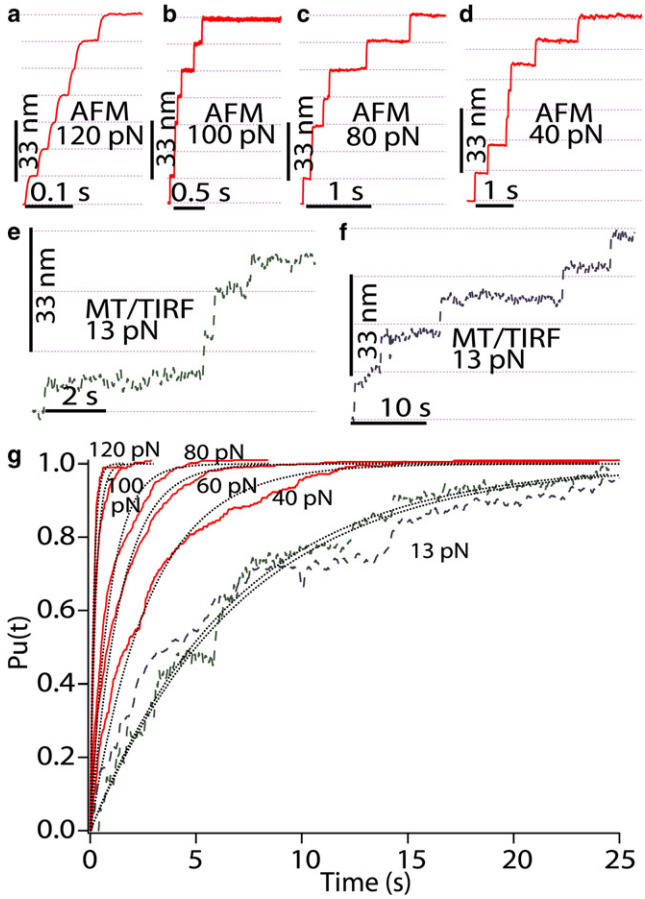

FIGURE 6 Typical length-versus-time recordings of a concatamer of $(\text{Protein L})_8$ stretched at (*a*) 120 pN, (*b*) 100 pN, (*c*) 80 pN, and (*d*) 40 pN, with a force-clamp AFM set-up, and at (*e*, *f*) ~13 pN with electromagnetic tweezers, yielding staircases in which every single step corresponds to the unfolding of a single module in the polyprotein chain. As it is apparent from the traces, the unfolding time is reduced as the pulling force is increased, and the step height increases with the stretching force. (*g*) Six averaged and normalized polyProtein L unfolding time courses obtained at different stretching forces: 13 pN, 40 pN, 60 pN, 80 pN, 100 pN, and 120 pN. Discontinuous black lines correspond to single exponential fits with rate constants presented in Fig. 7 *a*.

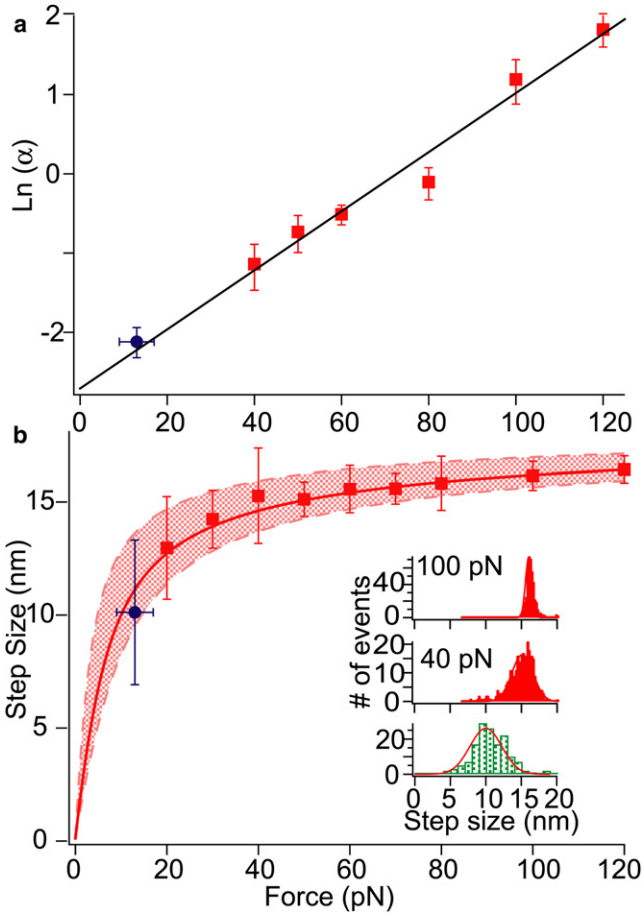

FIGURE 7 The unfolding rate of Protein L and the step height distribution at low unfolding forces measured with electromagnetic tweezers is consistent with the protein behavior in the high-force regime obtained with AFM. (*a*) Plot of the logarithm of the unfolding rate constant as a function of the pulling force for protein L obtained with AFM in the high-force regime (*solid squares*) and with electromagnetic tweezers in the low-force regime (*solid circle*). Linear fit of Eq. 6 in the text yields $\Delta x = 1.5 \pm 0.1$ Å and $\alpha(0) = 0.067 \pm 0.019\ s^{-1}$. (*b*) Plot of the step height distribution as a function of the pulling force. The fit of the WLC model of polymer elasticity (*solid line*) yields a contour length value of $L = 18.6$ nm and a persistence length value of $p = 0.58$ nm. The fits of the WLC to the experimental data where the persistence length is constrained to $p = 0.4$ nm and $p = 1.2$ nm (*dashed lines*) define a shaded region that captures the experimental step height distribution measured within a wide range of forces. (*Inset*) Histogram distribution of step heights at three different forces (13 pN, 40 pN, and 100 pN).

force. According to such predictions, obtaining the intrinsic unfolding rate in the absence of force from the extrapolation of the forced-unfolding data would result in an underestimation of the rate while the opposite trend is experimentally measured. The extrapolation of the rate constant in the absence of force, $\alpha(0) = 0.067\ s^{-1}$, is similar to that obtained from constant-velocity experiments ($\alpha(0) = 0.05\ s^{-1}$) and, as stated in Brockwell et al. (40), faster than the estimates for the unfolding rate in the absence of denaturants measured by different experimental methods (36,55). Such discrepancy in the $\alpha(0)$ value measured with both mechanical and chemical denaturing methods is not surprising, because it has been widely reported that the mechanical unfolding of proteins samples a totally different energy landscape than that probed by chemical or thermal denaturation (31,56).

Regarding the slope of the force-dependent unfolding kinetics obtained in the force-clamp mode, the measured value of $\Delta x = 1.5$ Å is shorter than the value reported by force-extension experiments, $\Delta x = 2.2$ Å (40). Interestingly, the same trend is also observed for ubiquitin and I27 (15,16). In constant velocity experiments, the force and the loading rate experienced by the molecule change over wide ranges on short timescales. Therefore, the quantification of the kinetic force-dependent parameters such as the unfolding rate in the absence of force, $\alpha(0)$, and the distance to the transition state, Δx, had to be done using highly simplified

Monte Carlo models, yielding only rough estimates. By contrast, force-clamp allows for a direct and precise measure of the force dependency of the unfolding reaction. The value of $\Delta x = 1.5$ Å measured here is of the same order of magnitude (~1–3 Å) as the distances to the transition state for a great variety of proteins measured with AFM (57), even when they are pulled from different directions (58–60). However, recent experiments with T4 lysozyme and maltose binding protein in constant velocity mode have reported slightly bigger distances to the transition state, ranging from 2 Å to 23 Å (61,62). In any case, the short distance to the transition state value measured here for protein L, $\Delta x = 1.5$ Å, is in sharp contrast to the distance to the unfolding transition state measured in RNase H using optical tweezers (23), for which $\Delta x = 20 \pm 1$ Å. Structurally, RNase H is an α-helix protein, different from the α-β fold of protein L. These topological differences may partially account for the 10-fold larger distance to the transition state measured for RNase H than for Protein L when pulled by optical and magnetic tweezers, respectively. However, it is also possible that the long DNA handles used in the optical tweezers set-up may also contribute to an overestimation of the measured Δx value (63).

One of the current limitations of our electromagnetic tweezers set-up lies in the fact that the pulling force exerted on the bead-protein system cannot be precisely set a priori during the experiment, because we do not have accurate control on the position of the bead with respect to the tip of our magnet. Given that the strength of the magnetic field changes along three spatial directions, it is only after in situ calibration (see Materials and Methods) that we can precisely assess the force at which the protein was pulled during each particular trajectory. This experimental constraint implies that in our ensemble of unfolding trajectories pulled at ~13 pN, we combine individual unfolding trajectories where each individual polyprotein is pulled at a particular force ranging from ~7 pN to ~19 pN. Such a pulling force range is reflected in the error bars of the unfolding rate and step height measurements at low-force regime (Fig. 7, *solid circle*). Such variability in the mean pulling force would entail significant uncertainty in the measured unfolding rate in the case of proteins exhibiting a large distance to the transition state such as RNase H, for which $\Delta x = 20 \pm 1$ Å. However, the unfolding rate of protein L is far less sensitive to the pulling force, $\Delta x = 1.5$ Å, and therefore the uncertainty in the unfolding rate is small. Indeed, a variability of 12 pN in the mean pulling force would imply an increase of unfolding rate of only 1.5 times for protein L. By contrast, the same variability in the pulling force for RNase H would result in a 300-fold change in the measured unfolding rate. Designing an experimental scheme to localize and control in situ the position of the magnetic bead with respect to the magnet tip would be a great improvement in the technique, because it would allow us to externally set the desired pulling force throughout the experiment. Although our electromagnet-based set-up produces lower magnetic fields than typical configurations based on permanent magnets, it has the advantage that it allows us to apply different force-pulse protocols to the protein within a short timescale, only by changing the externally applied current. Such experimental flexibility permits design of different force-pulse protocols to directly manipulate the conformational status of the protein. Furthermore, it avoids the mechanical hysteresis associated with the movement of the magnet, and it also has the potential capability of manipulating several beads simultaneously because of the bigger area of field. In any case, the lower magnetic fields provide experimental access to the low-force regime, which constitutes the main goal of this work.

In summary, we have shown the success of the combination of TIRF microscopy with the newly developed electromagnetic tweezers set-up to monitor the unfolding trajectories of a single protein under the effect of a constant pulling force. Although this technique does not reach the force sensitivity of optical tweezers, it constitutes a novel experimental way to study the behavior of mechanically stable proteins in the low-force regime without the need of linkage to long DNA handles or feedback loops for force adjustments. Future development of our experimental set-up will be focused on improving the electromagnetic tweezers to work at higher pulling forces and the chemical attachment of the protein between the magnetic bead and the glass surface, which would help increase the low protein pick-up ratio of our experiments. Altogether, the technique presented in this study provides an attractive experimental single-molecule approach that complements the well-established optical tweezers and AFM techniques. Furthermore, the absence of sensitivity to drift in the single-molecule recordings, which allows for the study of the same molecule for long periods of >1 h, provides new experimental avenues to test the evolution of the mechanical properties of proteins over time, such as aging effects. The capability of the evanescent nanometry technique to explore the low-force unfolding regime provides an ideal complement to force-clamp AFM to expand the accessible regions of the unfolding energy landscape of a mechanically stable protein. As a proof of principle, we show that the unfolding rate of the small protein L, which exhibits intermediate mechanical stability, is exponentially dependent with the pulling force down to ~13 pN, thereby excluding the presence of curvature in the rate-versus-force plot. Furthermore, the distribution of unfolding step height as a function of the pulling force is in very good agreement with the results obtained by force-ramp experiments, further validating the results obtained with this novel experimental approach. The development of hybrid single-molecule techniques where fluorescence is used as readout for the effects of a mechanical force applied to a molecule (33,64) promise to bring a degree of resolution of molecular dynamics, unattainable by each individual technique.

We thank Lorna Dougan for critical reading of the manuscript. S.G.-M. thanks the Generalitat de Catalunya for a postdoctoral fellowship through the NANO and Beatriu de Pinós programs, and also the Fundación Caja Madrid for financial support.

This work was supported by National Institutes of Health (grants HL66030 and HL61228 to J.M.F.).

REFERENCES

1. Carrion-Vazquez, M., P. E. Marszalek, A. F. Oberhauser, and J. M. Fernandez. 1999. Atomic force microscopy captures length phenotypes in single proteins. *Proc. Natl. Acad. Sci. USA*. 96:11288–11292.
2. Walther, K. A., J. Brujic, H. Li, and J. M. Fernandez. 2006. Sub-angstrom conformational changes of a single molecule captured by AFM variance analysis. *Biophys. J.* 90:3806–3812.
3. Dietz, H., and M. Rief. 2004. Exploring the energy landscape of GFP by single-molecule mechanical experiments. *Proc. Natl. Acad. Sci. USA*. 101:16192–16197.
4. Rief, M., M. Gautel, F. Oesterhelt, J. M. Fernandez, and H. E. Gaub. 1997. Reversible unfolding of individual titin immunoglobulin domains by AFM. *Science*. 276:1109–1112.
5. Rief, M., J. Pascual, M. Saraste, and H. E. Gaub. 1999. Single molecule force spectroscopy of spectrin repeats: low unfolding forces in helix bundles. *J. Mol. Biol.* 286:553–561.
6. Oberhauser, A. F., C. Badilla-Fernandez, M. Carrion-Vazquez, and J. M. Fernandez. 2002. The mechanical hierarchies of fibronectin observed with single-molecule AFM. *J. Mol. Biol.* 319:433–447.
7. Reference deleted in proof.
8. Li, H., A. F. Oberhauser, S. D. Redick, M. Carrion-Vazquez, H. P. Erickson, et al. 2001. Multiple conformations of PEVK proteins detected by single-molecule techniques. *Proc. Natl. Acad. Sci. USA*. 98:10682–10686.
9. Li, H., W. A. Linke, A. F. Oberhauser, M. Carrion-Vazquez, J. G. Kerkvliet, et al. 2002. Reverse engineering of the giant muscle protein titin. *Nature*. 418:998–1002.
10. Best, R. B., B. Li, A. Steward, V. Daggett, and J. Clarke. 2001. Can non-mechanical proteins withstand force? Stretching barnase by atomic force microscopy and molecular dynamics simulation. *Biophys. J.* 81:2344–2356.
11. Cao, Y., C. Lam, M. Wang, and H. Li. 2006. Nonmechanical protein can have significant mechanical stability. *Angew. Chem. Int. Ed. Engl.* 45:642–645.
12. Schwaiger, I., C. Sattler, D. R. Hostetter, and M. Rief. 2002. The myosin coiled-coil is a truly elastic protein structure. *Nat. Mater.* 1:232–235.
13. Ainavarapu, S. R., J. Brujic, H. H. Huang, A. P. Wiita, H. Lu, et al. 2007. Contour length and refolding rate of a small protein controlled by engineered disulfide bonds. *Biophys. J.* 92:225–233.
14. Oberhauser, A. F., P. K. Hansma, M. Carrion-Vazquez, and J. M. Fernandez. 2001. Stepwise unfolding of titin under force-clamp atomic force microscopy. *Proc. Natl. Acad. Sci. USA*. 98:468–472.
15. Schlierf, M., H. Li, and J. M. Fernandez. 2004. The unfolding kinetics of ubiquitin captured with single-molecule force-clamp techniques. *Proc. Natl. Acad. Sci. USA*. 101:7299–7304.
16. Garcia-Manyes, S., J. Brujic, C. L. Badilla, and J. M. Fernandez. 2007. Force-clamp spectroscopy of single-protein monomers reveals the individual unfolding and folding pathways of I27 and ubiquitin. *Biophys. J.* 93:2436–2446.
17. Liphardt, J., B. Onoa, S. B. Smith, I. J. Tinoco, and C. Bustamante. 2001. Reversible unfolding of single RNA molecules by mechanical force. *Science*. 292:733–737.
18. Onoa, B., S. Dumont, J. Liphardt, S. B. Smith, I. Tinoco, Jr, et al. 2003. Identifying kinetic barriers to mechanical unfolding of the *T. thermophila* ribozyme. *Science*. 299:1892–1895.
19. Gore, J., Z. Bryant, M. Nollmann, M. U. Le, N. R. Cozzarelli, et al. 2006. DNA overwinds when stretched. *Nature*. 442:836–839.
20. Woodside, M. T., W. M. Behnke-Parks, K. Larizadeh, K. Travers, D. Herschlag, et al. 2006. Nanomechanical measurements of the sequence-dependent folding landscapes of single nucleic acid hairpins. *Proc. Natl. Acad. Sci. USA*. 103:6190–6195.
21. Woodside, M. T., P. C. Anthony, W. M. Behnke-Parks, K. Larizadeh, D. Herschlag, et al. 2006. Direct measurement of the full, sequence-dependent folding landscape of a nucleic acid. *Science*. 314:1001–1004.
22. Cecconi, C., E. A. Shank, F. W. Dahlquist, S. Marqusee, and C. Bustamante. 2008. Protein-DNA chimeras for single molecule mechanical folding studies with the optical tweezers. *Eur. Biophys. J.* 37:729–738.
23. Cecconi, C., E. A. Shank, C. Bustamante, and S. Marqusee. 2005. Direct observation of the three-state folding of a single protein molecule. *Science*. 309:2057–2060.
24. Bechtluft, P., R. G. van Leeuwen, M. Tyreman, D. Tomkiewicz, N. Nouwen, et al. 2007. Direct observation of chaperone-induced changes in a protein folding pathway. *Science*. 318:1458–1461.
25. Greenleaf, W. J., M. T. Woodside, and S. M. Block. 2007. High-resolution, single-molecule measurements of biomolecular motion. *Annu. Rev. Biophys. Biomol. Struct.* 36:171–190.
26. Neuman, K. C., and A. Nagy. 2008. Single-molecule force spectroscopy: optical tweezers, magnetic tweezers and atomic force microscopy. *Nat. Methods*. 5:491–505.
27. Charvin, G., T. R. Strick, D. Bensimon, and V. Croquette. 2005. Tracking topoisomerase activity at the single-molecule level. *Annu. Rev. Biophys. Biomol. Struct.* 34:201–219.
28. Strick, T. R., V. Croquette, and D. Bensimon. 2000. Single-molecule analysis of DNA uncoiling by a type II topoisomerase. *Nature*. 404:901–904.
29. Gore, J., Z. Bryant, M. D. Stone, M. Nollmann, N. R. Cozzarelli, et al. 2006. Mechanochemical analysis of DNA gyrase using rotor bead tracking. *Nature*. 439:100–104.
30. Itoh, H., A. Takahashi, K. Adachi, H. Noji, R. Yasuda, et al. 2004. Mechanically driven ATP synthesis by F1-ATPase. *Nature*. 427:465–468.
31. West, D. K., P. D. Olmsted, and E. Paci. 2006. Mechanical unfolding revisited through a simple but realistic model. *J. Chem. Phys.* 124:154909.
32. Williams, P. M., S. B. Fowler, R. B. Best, J. L. Toca-Herrera, K. A. Scott, et al. 2003. Hidden complexity in the mechanical properties of titin. *Nature*. 422:446–449.
33. Sarkar, A., R. B. Robertson, and J. M. Fernandez. 2004. Simultaneous atomic force microscope and fluorescence measurements of protein unfolding using a calibrated evanescent wave. *Proc. Natl. Acad. Sci. USA*. 101:12882–12886.
34. Gu, H., D. Kim, and D. Baker. 1997. Contrasting roles for symmetrically disposed β-turns in the folding of a small protein. *J. Mol. Biol.* 274:588–596.
35. Kim, D. E., C. Fisher, and D. Baker. 2000. A breakdown of symmetry in the folding transition state of protein L. *J. Mol. Biol.* 298:971–984.
36. Scalley, M. L., Q. Yi, H. Gu, A. McCormack, J. R. Yates, 3rd, et al. 1997. Kinetics of folding of the IgG binding domain of peptostreptococcal protein L. *Biochemistry*. 36:3373–3382.
37. Scalley, M. L., and D. Baker. 1997. Protein folding kinetics exhibit an Arrhenius temperature dependence when corrected for the temperature dependence of protein stability. *Proc. Natl. Acad. Sci. USA*. 94:10636–10640.
38. Merchant, K. A., R. B. Best, J. M. Louis, I. V. Gopich, and W. A. Eaton. 2007. Characterizing the unfolded states of proteins using single-molecule FRET spectroscopy and molecular simulations. *Proc. Natl. Acad. Sci. USA*. 104:1528–1533.
39. Sherman, E., and G. Haran. 2006. Coil-globule transition in the denatured state of a small protein. *Proc. Natl. Acad. Sci. USA*. 103:11539–11543.

40. Brockwell, D. J., G. S. Beddard, E. Paci, D. K. West, P. D. Olmsted, et al. 2005. Mechanically unfolding the small, topologically simple protein L. *Biophys. J.* 89:506–519.

41. Carrion-Vazquez, M., A. F. Oberhauser, S. B. Fowler, P. E. Marszalek, S. E. Broedel, et al. 1999. Mechanical and chemical unfolding of a single protein: a comparison. *Proc. Natl. Acad. Sci. USA.* 96:3694–3699.

42. Reference deleted in proof.

43. Fernandez, J. M., and H. Li. 2004. Force-clamp spectroscopy monitors the folding trajectory of a single protein. *Science.* 303:1674–1678.

44. Florin, E. L., M. Rief, H. Lehmann, M. Ludwig, C. Dornmair, et al. 1995. Sensing specific molecular-interactions with the atomic-force microscope. *Biosens. Bioelectron.* 10:895–901.

45. Reference deleted in proof.

46. Kreuzer, H. J., S. H. Payne, and L. Livadaru. 2001. Stretching a macromolecule in an atomic force microscope: statistical mechanical analysis. *Biophys. J.* 80:2505–2514.

47. Brujic, J., R. I. Hermans, S. Garcia-Manyes, K. A. Walther, and J. M. Fernandez. 2007. Dwell-time distribution analysis of polyprotein unfolding using force-clamp spectroscopy. *Biophys. J.* 92:2896–2903.

48. Brujic, J., R. I. Hermans, K. A. Walther, and J. M. Fernandez. 2006. Single-molecule force spectroscopy reveals signatures of glassy dynamics in the energy landscape of ubiquitin. *Nat. Phys.* 2:282–286.

49. Cao, Y., R. Kuske, and H. Li. 2008. Direct observation of Markovian behavior of the mechanical unfolding of individual proteins. *Biophys. J.* 95:782–788.

50. Dougan, L., G. Feng, H. Lu, and J. M. Fernandez. 2008. Solvent molecules bridge the mechanical unfolding transition state of a protein. *Proc. Natl. Acad. Sci. USA.* 105:3185–3190.

51. Bell, G. I. 1978. Models for the specific adhesion of cells to cells. *Science.* 200:618–627.

52. Reference deleted in proof.

53. Walther, K. A., F. Grater, L. Dougan, C. L. Badilla, B. J. Berne, et al. 2007. Signatures of hydrophobic collapse in extended proteins captured with force spectroscopy. *Proc. Natl. Acad. Sci. USA.* 104:7916–7921.

54. Reference deleted in proof.

55. Yi, Q., M. L. Scalley, K. T. Simons, S. T. Gladwin, and D. Baker. 1997. Characterization of the free energy spectrum of peptostreptococcal protein L. *Fold. Des.* 2:271–280.

56. Fowler, S. B., R. B. Best, J. L. Toca Herrera, T. J. Rutherford, A. Steward, et al. 2002. Mechanical unfolding of a titin Ig domain: structure of unfolding intermediate revealed by combining AFM, molecular dynamics simulations, NMR and protein engineering. *J. Mol. Biol.* 322:841–849.

57. Carrion-Vazquez, M., A. F. Oberhauser, H. Diez, R. Hervas, J. Oroz, et al. 2006. Protein nanomechanics, as studied by AFM single-molecule force spectroscopy. *In* Advanced Techniques in Biophysics. J. L. R Arrondo and A. Alonso, editors. Springer-Verlag, Heidelberg, pp. 163–245.

58. Carrion-Vazquez, M., H. Li, H. Lu, P. E. Marszalek, A. F. Oberhauser, et al. 2003. The mechanical stability of ubiquitin is linkage dependent. *Nat. Struct. Biol.* 10:738–743.

59. Brockwell, D. J., E. Paci, R. C. Zinober, G. S. Beddard, P. D. Olmsted, et al. 2003. Pulling geometry defines the mechanical resistance of a beta-sheet protein. *Nat. Struct. Biol.* 10:731–737.

60. Dietz, H., F. Berkemeier, M. Bertz, and M. Rief. 2006. Anisotropic deformation response of single protein molecules. *Proc. Natl. Acad. Sci. USA.* 103:12724–12728.

61. Peng, Q., and H. Li. 2008. Atomic force microscopy reveals parallel mechanical unfolding pathways of T4 lysozyme: evidence for a kinetic partitioning mechanism. *Proc. Natl. Acad. Sci. USA.* 105:1885–1890.

62. Bertz, M., and M. Rief. 2008. Mechanical unfoldons as building blocks of maltose-binding protein. *J. Mol. Biol.* 378:447–458.

63. West, D. K., E. Paci, and P. D. Olmsted. 2006. Internal protein dynamics shifts the distance to the mechanical transition state. *Phys. Rev. E Stat. Nonlin. Soft Matter Phys.* 74:061912.

64. Hohng, S., R. Zhou, M. K. Nahas, J. Yu, K. Schulten, et al. 2007. Fluorescence-force spectroscopy maps two-dimensional reaction landscape of the holliday junction. *Science.* 318:279–283.